Biosensors and Bioelectronics 94 (2017) 478–484

Contents lists available at ScienceDirect

Biosensors and Bioelectronics

journal homepage: www.elsevier.com/locate/bios

Label-free silicon nanodots featured ratiometric fluorescent aptasensor for lysosomal imaging and pH measurement

Yanan Zhang, Shan Guo, Shibo Cheng, Xinghu Ji*, Zhike He*

Key Laboratory of Analytical Chemistry for Biology and Medicine (Ministry of Education), College of Chemistry and Molecular Sciences, Wuhan University, Wuhan 430072, China

ARTICLE INFO

Keywords:
Silicon nanodots
Aptasensor
Fluorescence imaging
Lysosomal pH

ABSTRACT

The homeostasis of lysosomal pH is crucial in cell physiology. Developing small fluorescent nanosensors for lysosome imaging and ratiometric measurement of pH is highly demanded yet challenging. Herein, a pH-sensitive fluorescein tagged aptamer AS1411 has been utilized to covalently modify the label-free fluorescent silicon nanodots via a crosslinker for construction of a ratiometric pH biosensor. The established aptasensor exhibits the advantages of ultrasmall size, hypotoxicity, excellent pH reversibility and good photostability, which favors its application in an intracellular environment. Using human breast MCF-7 cancer cells and MCF-10A normal cells as the model, this aptasensor shows cell specificity for cancer cells and displays a wide pH response range of 4.5–8.0 in living cells. The results demonstrate that the pH of MCF-7 cells is 5.1, which is the expected value for acidic organelles. Lysosome imaging and accurate measurement of pH in MCF-7 cells have been successfully conducted based on this nanosensor via fluorescent microscopy and flow cytometry.

1. Introduction

Hydrogen ions are a vital species in cells and intracellular distribution of hydrogen ions is uneven in the subcellular compartments (Han and Burgess, 2010; Casey et al., 2010). Usually, mitochondria possess a basic pH of about 8.0 (Chen et al., 2015; Wu et al., 2015), the pH in cytoplasm and nucleus is typically 7.2–7.4 (Pan et al., 2016; Shi et al., 2012), Lysosome, as one of the key organelles, has an acidic pH ranging from 4.7 to 5.5 (Bao et al., 2015; Gong et al., 2014; Marin et al., 2012). Lysosome plays a pivotal role in cellular homeostasis, such as plasma membrane repair, protein degradation, and certain pathogens removal (Turk and Turk, 2009). Disturbances of the lysosomal pH have been associated with autophagy block, lysosomal degradation ability reduction and storage disorders (Vidal-Donet et al., 2013). Moreover, the drug delivery systems for treatment of tumor cells are associated with pH measurement (Ji et al., 2015). Therefore, accurate measurement of hydrogen ions in lysosomes is of great significance to gain insight into the cellular behavior.

The last decades have witnessed a great advance in ratiometric fluorescent nanosensors for the sensing and quantification of biological analytes (Zhao et al., 2009; Chen et al., 2014; Wan et al., 2014). These nanosensors with dual emission signals have the function of self-calibration for the influences of analyte-independent factors, such as excitation source fluctuations, probe concentration, optical path length, or leakage from the cells (Han and Burgess, 2010). Various optical chemical nanosensors have been designed for ratiometric measurement of intracellular pH based on carbon dots (Nie et al., 2014; Shangguan et al., 2016; Shi et al., 2012), silica nanoparticles (Pan et al., 2016), gold nanoparticles (Marin et al., 2012), polypeptide nanoparticles (Gong et al., 2014), quantum dots (Dennis et al., 2012), metal-organic frameworks (He et al., 2014), dendrimers (Albertazzi et al., 2010), and polymer nanoparticles (Bao et al., 2015; Chan et al., 2011). However, quite a few of these nanomaterials have no fluorescence themselves, and they are typically modified with two fluorophores (Scheme 1a) even the toxic ethidium bromide, which requires a relatively complicated process of synthesis and exists safety risk (Bao et al., 2015; Gong et al., 2014; Marin et al., 2012; Pan et al., 2016). Some fluorescent nanoparticles (NPs) can act as both a signal reference and a nanocarrier (Scheme 1b), while the heavy-metal content in the Group II–VI fluorescent quantum dots (QDs) (Dennis et al., 2012), may not facilitate their application in an intracellular environment. The fluorescent sensors utilized for lysosomal imaging typically possess a diameter of 4–100 nm, it may be concluded that NPs smaller than ~100 nm usually can penetrate the cell membrane (Bao et al., 2015; Ji et al., 2015; Pan et al., 2016). Thus, a more stable, environmental-friendly, easily synthesized, ultrasmall fluorescent nanomaterial is urgent to be developed. Fluorescent silicon nanocrystals, also known as silicon QDs, are emerging as an attractive class of nanoparticles, due

* Corresponding authors.
E-mail address: zhkhe@whu.edu.cn (Z. He).

http://dx.doi.org/10.1016/j.bios.2017.03.041
Received 3 February 2017; Received in revised form 14 March 2017; Accepted 19 March 2017
Available online 22 March 2017

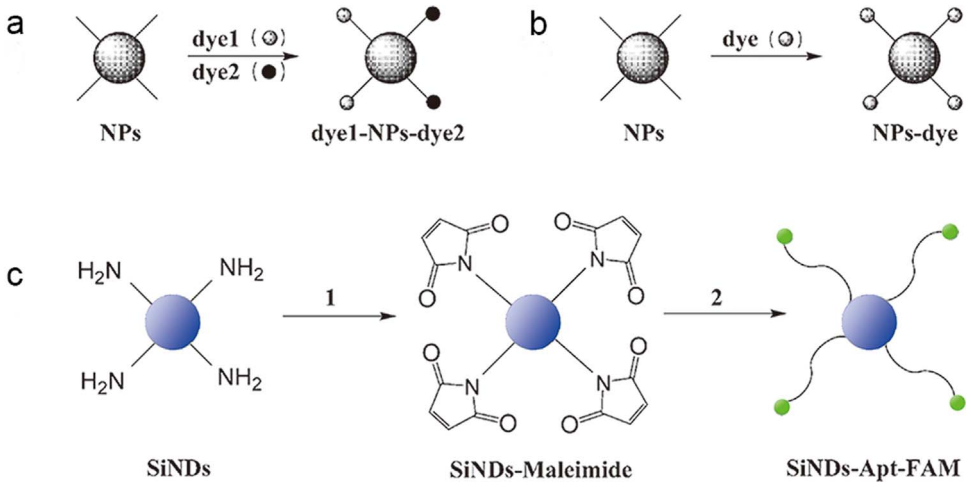

Scheme 1. (a) Two dyes used for construction of ratiometric sensors based on nonfluorescent NPs. (b) One dye used for construction of ratiometric sensors based on fluorescent NPs. (c) Preparation of fluorescein tagged aptamer-modified SiNDs (SiNDs-Apt-FAM). 1, Sulf-SMCC, pH 7.4, 0.5 h; 2, FAM-DNA-SH, pH 6.8, overnight.

to the abundant silicon in the Earth's crust and their hypotoxicity compared to lots of other QDs (II–VI and III–V, etc.) (Dasog et al., 2016). Most recent results demonstrated that silicon nanoparticles exhibited good photostability in a physiological environment and their biodegradation product could be excreted through the urine (Gu et al., 2013; Montalti et al., 2015; Wang et al., 2014; Zhong et al., 2015). And among the reported pH nanosensors, silica-based sensor (up to 2 mg mL^{-1}) (Pan et al., 2016) displayed better biocompatibility than the sensor based on polypeptide nanoparticles (up to 20 μg mL^{-1}) (Gong et al., 2014) through cytotoxicity assay. To the best of our knowledge, silicon QDs can be a good alternative for fluorescence imaging in living cells and construction of a ratiometric pH biosensor.

Label-free fluorescent silicon nanodots (SiNDs) with amino-terminated surface has been synthesized via a facile hydrothermal method in our previous work (Feng et al., 2014). And a highly sensitive pH sensor was developed using the SiNDs as a single emission signal for determination of pH values of water samples. The property of the SiNDs integrating good water-solubility, high photostability (approximately stabilized within 30 min irradiated by a Xe lamp), strong fluorescence, as well as long lifetime (6.199 ns) (Feng et al., 2014) makes it suitable for developing a ratiometric pH biosensor. Herein, we selected a biocompatible aptamer AS1411 (Apt) as a ligand to covalently functionalize the SiNDs via the crosslinker Sulfo-SMCC reagent (Scheme 1c). AS1411 was a guanosine-rich DNA aptamer that bound specifically to nucleolin, a protein overexpressed on the plasma membrane of cancer cells (e.g., MCF-7 and HeLa cells) (Cao et al., 2013; Zhang et al., 2014; Zhou et al., 2015). The amino groups of SiNDs fully reacted with the succinimide of excess Sulfo-SMCC and the product SiNDs-Maleimide acted as a pH-insensitive fluorescence reference. Then, the aptamer AS1411 modified with a pH-sensitive fluorescein (FAM) at one end and the sulfhydryl group (-SH) at the other end was used to react with the SiNDs-Maleimide through Michael reaction (Wang et al., 2016). The covalent functionalization of SiNDs facilitates the application for intracellular sensing. Recent studies have shown that incorporation of the aptamer AS1411 adds targeting ability and also enhances cellular uptake through the nucleolin-mediated endocytosis, making it an appropriate ligand for targeting cancer cells and delivering drugs (Li et al., 2012, 2015; Liu et al., 2016; Qiu et al., 2013; Shieh et al., 2010; Wang et al., 2016). We confirmed that the established ratiometric pH aptasensor (SiNDs-Apt-FAM) displayed cell specificity for MCF-7 cancer cells with nucleolin highly expressed in comparison with MCF-10A normal cells.

Combination of fluorescent microscopy with flow cytometry techniques has notably proved to be an effective approach for obtaining both spatial information and quantitative analysis at the molecular level (Chen et al., 2015). Fluorescent microscopy provided significant information concerning the spatially-resolved distribution of SiNDs-Apt-FAM throughout the cell. The specific accumulation of SiNDs-Apt-FAM in lysosomes was probably due to the interaction of the aptasensor with nucleolin that was highly expressed in MCF-7 cells and the subsequent nucleolin-mediated internalization (Shieh et al., 2010). In the reported methods, owing to the high-throughput characterization of thousands of individual cells, flow cytometry was a more convenient and reliable method for quantitative multispectral analysis than confocal microscopy (Chen et al., 2015; Patrick et al., 2013). Chen and co-workers (Chen et al., 2015) developed a fluorescein/cyanine hybrid sensor for ratiometric detection of pH in mitochondria via fluorescence imaging and flow cytometry. Patrick and co-workers (Patrick et al., 2013) designed unique perfluorocarbon nanoemulsions enabling intracellular pH measurement by flow cytometry. In this work, flow cytometry offered great convenience for simultaneous multispectral analysis of SiNDs-Apt-FAM in living cells. Lysosome imaging and quantitative analysis of hydrogen ions have been performed based on this new ratiometric fluorescent aptasensor.

2. Experimental

2.1. Reagents and materials

4-(N-Maleimidomethyl)cyclohexane-1-carboxylic acid 3-sulfo-N-hydroxysuccinimide ester sodium salt (Sulfo-SMCC), 3-(4,5-dimethyl-2-thiazoyl)-2,5-diphenyl tetrazolium bromide (MTT), dimethylsulfoxide (DMSO), nigericin sodium salt, Dulbecco's Modified Eagle's Medium-high glucose (DMEM) were purchased from Sigma-Aldrich Trading Co., Ltd (Shanghai, China). LysoTracker Red DND-99 (Life Technologies, USA) was used for subcellular localization. All of the other essential chemicals were of analytical grade, unless otherwise stated. High purity water (18.2 MΩ cm) obtained from Milli-Q Element system (Millpore Co. Ltd, U.S.A.) was used throughout the experimental process. Before use, the aqueous solutions were filtered with a 0.22 μm membrane filter (Millpore. Co. Ltd, U.S.A.). HPLC purified oligonucleotides AS1411 were purchased from Sangon Biotech Co., Ltd (Shanghai, China). The sequences of the oligonucleotide used in this work were listed as followed:

Apt-linker-0A: 5'-FAM-GGT GGT GGT GGT TGT GGT GGT GGT GG-(C3)SH-3'
Apt-linker-6A: 5'-FAM-GGT GGT GGT GGT TGT GGT GGT GGT GGAAAAAA-(C3)SH-3'
Apt-linker-8A: 5'-FAM-GGT GGT GGT GGT TGT GGT GGT GGT

GGAAAAAAAA-(C3)SH-3'
Apt-linker-10A: 5'-FAM-GGT GGT GGT GGT TGT GGT GGT GGT GGAAAAAAAAAA-(C3)SH 3'

2.2. Preparation of SiNDs-Apt-FAM

Preparation of SiNDs-Maleimide: label-free SiNDs were dispersed in phosphate buffered saline (PBS, pH 7.4, 150 mM NaCl) (200 mg mL^{-1}) by ultrasonication, followed by addition of 11.5 mM Sulfo-SMCC solution. The mixture (1 mL) was allowed to stand on a shaker (Essenscien V6, USA) for 0.5 h at room temperature to yield SiNDs-Maleimide. The product was obtained after washing three times (8500 rpm×10 min, per time) with the PBS buffer (pH 6.8, 150 mM NaCl) through the Amicon-3K filters by a Sorvall Legend Micro 17 R microcentrifuge (Thermo, USA).

Optimization of the linker length of aptamer: considering the steric hindrance between FAM-Apt-SH and SiNDs-Maleimide, the effect of the linker length of the aptamer was investigated. The aptamers (Apt-linker-0A, Apt-linker-6A, Apt-linker-8A, Apt-linker-10A) were primarily heated at 95 °C for 10 min in 28 mM Tris-HCl buffer (200 mM KCl, 4 mM $MgCl_2$) and then cooled to room temperature (Wang et al., 2016). The purified SiNDs-Maleimide solutions containing 13 mg SiNDs-Maleimide (calculated according to Fig. S1a) were incubated with various 100 μM annealed aptamers at room temperature overnight with gentle shaking, respectively. The aptamer-functionalized SiNDs were then washed with PBS (pH 7.4) for six times (8500 rpm×10 min, per time) through Amicon-10K filters. The SiNDs-aptamer-FAM with linker-8A shows the optimal fluorescence ratio (Fig. S2a).

Optimization of the ratio of FAM/SiNDs: optimization of the amount of SiNDs-Maleimide to react with Apt-linker-8A is essential in developing ratiometric nanosensors that are appropriate for platforms such as fluorescence microscopy or flow cytometry. The purified solution containing 13, 26, 39 and 52 mg SiNDs-Maleimide (calculated according to Fig. S1a) were added with 100 μM (10 nmol) FAM-Apt-SH, respectively. Then the solutions (0.5 mL) were shaken tenderly overnight at room temperature. After purification for six times, the fluorescence intensity of the solutions diluted to the same volume with ultrapure water were determined. The conjugation efficiency was calculated to be 0.44–0.61 nmol DNA per mg SiNDs (calculated according to Fig. S1) depending on the amount of SiNDs-Maleimide in the solution. The FAM to SiNDs signal ratios are in the range of 0.55–1.15. With a suitable ratio, the dual-emission signals of the SiNDs-Apt-FAM could be both enhanced so that the fluorescence of the nanosensor could largely distinguish from the autofluorescence of the living cells, which favors its application in the platforms of fluorescence microscopy and flow cytometry. As an optimized ratio, the SiNDs-Apt-FAM aptasensor prepared with 39 mg SiNDs-Maleimide (calculated according to Fig. S1a) and 10 nmol Apt-linker-8A was selected for the further experiments (Fig. S2b).

Characterization: The absorption spectra of the filtered solution were obtained on a UV-2550 spectrophotometer (Shimadzu). Zeta potential measurements were carried out on a Zetasizer nano ZS instrument (ZEN3600, Malvern, England). Transmission electron microscopy image (TEM) of the optimized SiNDs-Apt-FAM aptasensor was obtained on a JEM-2100 instrument (JEOL Ltd., Japan).

2.3. Fluorescence assays in aqueous solutions

Fluorescence emission spectra of the SiNDs-Apt-FAM aptasensor (400 μg mL^{-1}) in aqueous solutions were obtained on a fluorometer (RF-5301, Shimadzu) with the synchronous scan method (Ex =365 nm, scan range: 390–580 nm, slit widths of excitation and emission: (10 nm, 5 nm)) at ambient temperature.

2.4. Fluorescence imaging with SiNDs-Apt-FAM in living cells

MCF-7 cancer cells (1×10^4 cells/well) were grown on glass-bottom culture dishes (Nest Biotechnology Co. LTD.) in the DMEM media at 37 °C for 24 h in a 5% CO_2 incubator. The cells were then incubated with SiNDs-Apt-FAM (400 μg mL^{-1}) for 4 h in fresh DMEM media. Before use, MCF-7 cells were washed three times with PBS (pH 7.4) to remove the excess SiNDs-Apt-FAM. Cells incubated without SiNDs-Apt-FAM were treated the same procedure. MCF-10A normal cells (1×10^4 cells/well) were treated the same way. HeLa cells (1×10^4 cells/well) were also incubated under the same conditions. Fluorescence images were obtained via a Zeiss microscope (AxioObserver Z1, Zeiss, Germany) at 100× magnification from the fluorescence emitted by SiNDs-Apt-FAM.

2.5. Fluorescence ratiometric detection of lysosomal pH with SiNDs-Apt-FAM

MCF-7 cells (6×10^4 cells/well) were incubated 24 h in 6-well plates at 37 °C in a 5% CO_2 incubator. Cells were then treated by 400 μg mL^{-1} SiNDs-Apt-FAM for 4 h. Cells were rinsed with PBS three times, and then incubated in high K^+ buffer (30 mM NaCl, 120 mM KCl, 1 mM $CaCl_2$, 0.5 mM $MgSO_4$, 1 mM NaH_2PO_4, 5 mM glucose, 20 mM HEPES) with various pH values (4.5, 5.0, 6.0, 7.0, and 8.0) in the presence of 10 μM nigericin (Shi et al., 2012). After 30 min, plates were rinsed with buffer solutions three times and the cells were trypsinized, transferred to tubes and centrifuged at 1000 rpm for 6 min. The trypsin-contained medium in the supernatant was replaced with HEPES solutions. Then the well mixed solutions containing MCF-7 cells were analyzed directly by the flow cytometry (CyAn ADP, Beckman, USA). The experimental group (i.e., the cells were treated by SiNDS-Apt-FAM and then incubated 30 min in PBS buffer) and the control group (i.e., the cells were untreated by SiNDs-Apt-FAM and then incubated 30 min in PBS buffer) were treated the same way.

3. Results and discussion

3.1. Characterization of SiNDs-Apt-FAM

The absorbances of 265 nm and 337 nm were close to zero after purification for six times, demonstrating sufficient removal of free aptamers and SiNDs (Fig. S3a). FAM-Apt-SH conjugation on the surface of SiNDs was confirmed using zeta potential measurement. The zeta potential of SiNDs and SiNDs-Maleimide was 0.35 ± 0.05 and −4.25 ± 0.38 mV, respectively. After FAM-Apt-SH conjugation, the zeta potential of the SiNDs-Apt-FAM was −11.1 ± 1.1 mV (Fig. S3b). The negatively charged phosphate groups of FAM-Apt-SH are responsible for the negative shift of the zeta potential, indicating the successful conjugation of FAM-Apt-SH on the surface of SiNDs-Maleimide. Fig. S3c presents the TEM of the SiNDs-Apt-FAM which appears as spherical particles with good monodispersity. The size distribution shows that the aptasensor has an average diameter of 3.7 ± 0.7 nm (Fig. S3d), which is larger than that of pure SiNDs with an average diameter of about 2.5 nm (Feng et al., 2014), demonstrating that modification of the DNA aptamer changes the size of SiNDs.

3.2. Performance of SiNDs-Apt-FAM toward pH

The fluorescence spectra of SiNDs-Apt-FAM were examined in 20 mM phosphate buffered saline (PBS) solution with the synchronous scan method, which could offer multispectral data in a single measurement and was more simple, effective than the dual excitation mode utilized in the ratiometric fluorescence system (He et al., 2014; Patrick et al., 2013). As depicted in Fig. 1a, the fluorescence intensity ratio of FAM at 528 nm and SiNDs at 422 nm was increased gradually with the enhancement of pH values. And the SiNDs-Apt-FAM nanosensor

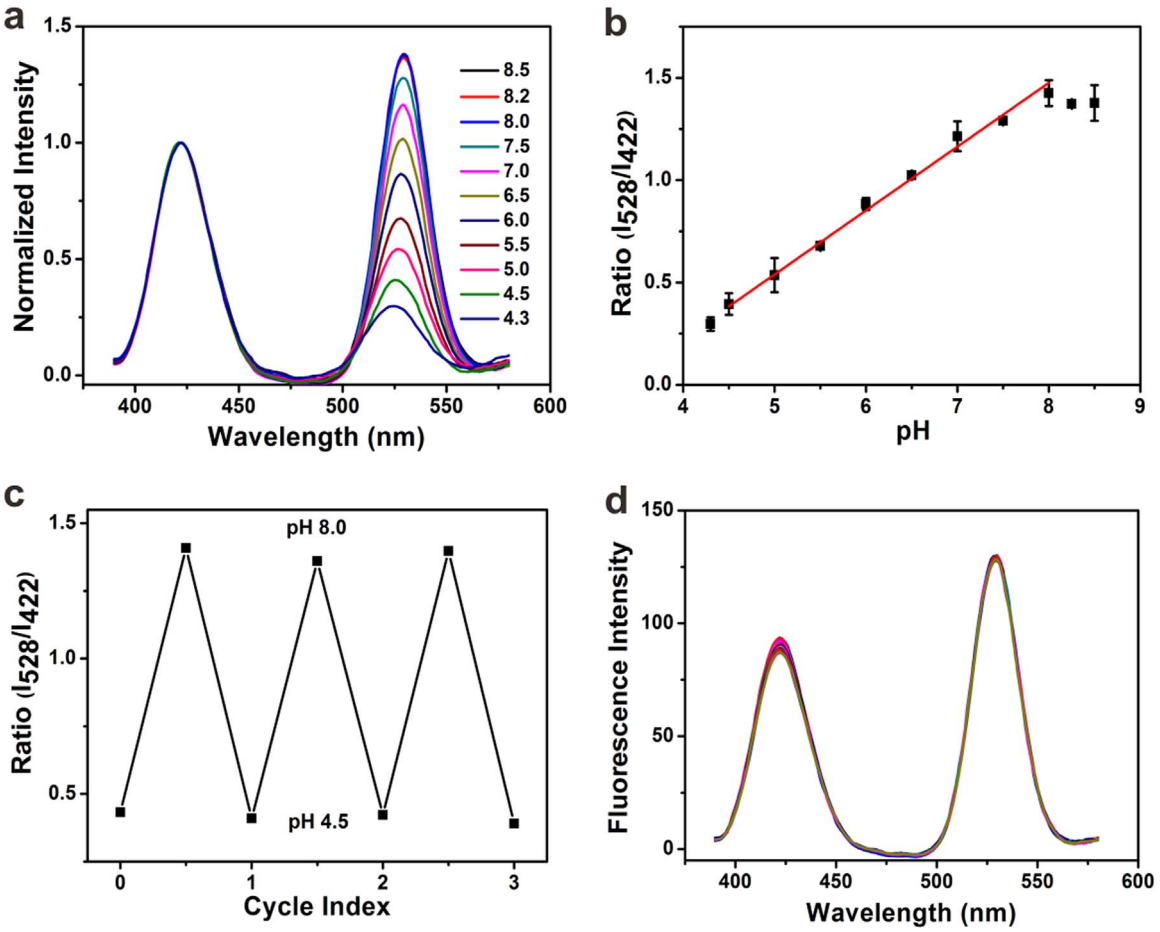

Fig. 1. (a) Fluorescence spectra of SiNDs-Apt-FAM (400 μg mL^{-1}) in 20 mM PBS at various pH. (b) Response range of SiNDs-Apt-FAM in 20 mM PBS at various pH. (c) Reversible fluorescence ratio (I_{528}/I_{422}) changes of SiNDs-Apt-FAM between pH 4.5 and 8.0. (d) Fluorescence changes of SiNDs-Apt-FAM with 20 times excitation.

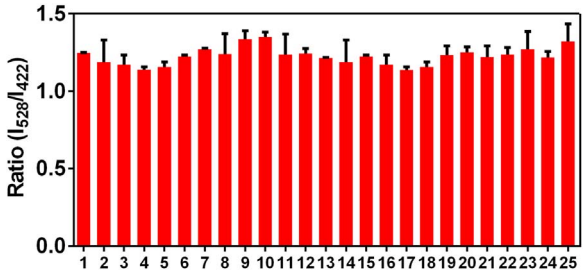

Fig. 2. Fluorescence intensity ratio (I_{528}/I_{422}) of SiNDs-Apt-FAM in the presence of different cations, biological species, and anions (1: blank; 2: 210 mM K^+; 3: 140 mM Na^+; 4: 1 mM Mn^{2+}; 5: 20 mM NH_4^+; 6: 2.5 mM Ca^{2+}; 7: 10 mM Mg^{2+}; 8: 0.125 mM Fe^{3+}; 9: 0.125 mM Zn^{2+}; 10: 0.125 mM Fe^{2+}; 11: 0.5 μM Cu^{2+}; 12: 20 mM Glucose; 13: 1 mM glutathione; 14: 210 mM Cl^-; 15: 10 mM SO_4^{2-}; 16: 140 mM NO_3^-; 17: 40 mM I^-; 18: 20 mM HCO_3^-; 19: 20 mM CO_3^{2-}; 20: 0.4 mM NO_2^-; 21: 40 mM F^-; 22: 40 mM Br^-; 23: 4 mM PO_4^{3-}; 24: 0.5 μM ClO^-; 25: 40 mM CH_3COO^-) in PBS buffer (20 mM, pH 7.4, 37 °C).

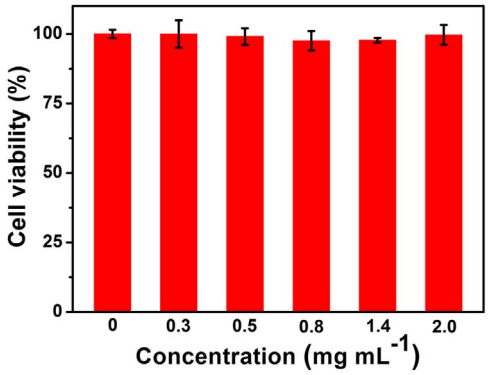

Fig. 3. Cell viability incubated with SiNDs-Apt-FAM at varied concentrations.

possessed a wide linear range of pH 4.3–8.0 [y=0.315x – 1.03, R^2=0.991] (Fig. 1b). To investigate the pH reversibility of this aptasensor, the solution of SiNDs-Apt-FAM (400 μg mL^{-1}) between pH 4.5 and pH 8.0 was adjusted with 2 M HCl or 2 M NaOH, and then measured by a PB-10 pH-meter (Sartorius, Germany) before fluorescence determination. This sensing process could be reversibly conducted for at least 3 cycles (Fig. 1c), indicating SiNDs-Apt-FAM was a highly reversible aptasensor for pH sensing. Then, a fluorescence stability study of the aptasensor in 20 mM PBS was conducted. The fluorescence intensity of 400 μg mL^{-1} SiNDs-Apt-FAM in the buffer solution was measured under multiple excitation by the synchronous scan method. As shown in Fig. 1d, the fluorescence emission spectra and the intensity ratio (I_{528}/I_{422}) of SiNDs-Apt-FAM remain constant after twenty times excitation. This aptasensor displays good photostability in aqueous solution.

The pK_a value for SiNDs-Apt-FAM was determined from the changes of the fluorescence intensity ratio with various pH values, using the modified Henderson–Hasselbalch equation (Kosegarten and Englisch, 1994):

$$\text{Log}\,[(R_{max}-R_I)/(R_I-R_{min})] = pK_a - pH \quad (1)$$

where R_I was the intensity ratio of SiNDs-Apt-FAM at various pH levels, and R_{max} and R_{min} were the corresponding maximum and minimum fluorescence ratio of the aptasensor, respectively. The pK_a

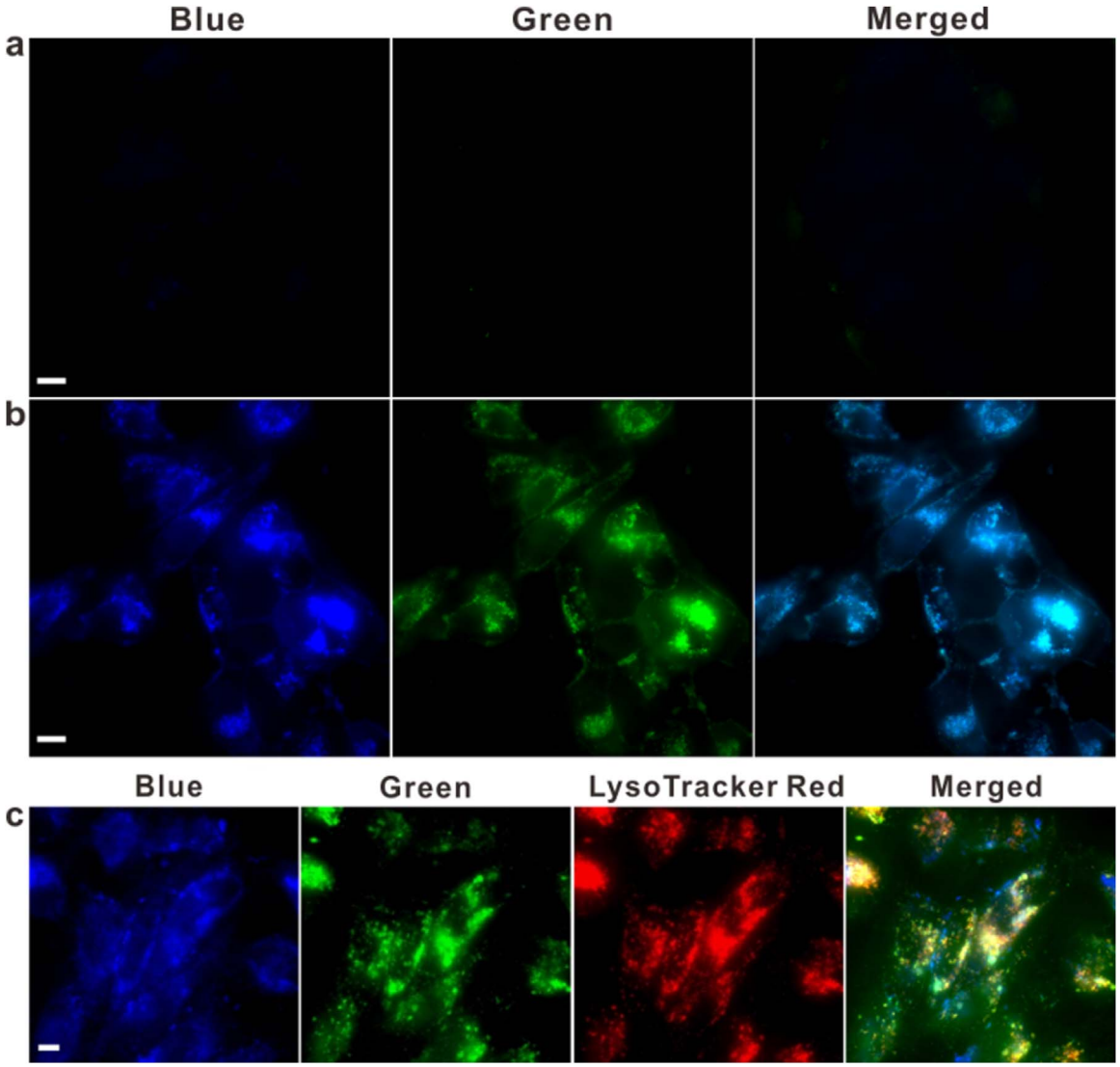

Fig. 4. Fluorescence images of (a) MCF-10A cells and (b) MCF-7 cells incubated with SiNDs-Apt-FAM, respectively. (c) Fluorescence images of MCF-7 cells incubated with SiNDs-Apt-FAM and LysoTracker Red DND-99. The images were collected in blue channel, green channel, and red channel, respectively, and merged images were shown as well. Scale bars: 20 μm. (For interpretation of the references to color in this figure legend, the reader is referred to the web version of this article.)

value of SiNDs-Apt-FAM was calculated to be 6.3 by calculating the ratios of fluorescence intensity at various pH values (Fig. S4). The SiNDs-Apt-FAM presents sensitive response to pH around the pK_a of fluorescein (6.4) (Xu et al., 2011), meaning the ratiometric pH aptasensor is suitable for fluorescence detection of pH in living cells (Wencel et al., 2014; Wu et al., 2016).

To further explore if this aptasensor could still work well in a relatively complex environments, some common ions and biomolecules were taken as the interference to test the response of SiNDs-Apt-FAM to proton. The effects of these intracellular species on the fluorescence response of SiNDs-Apt-FAM were investigated under physiological conditions (PBS, pH 7.4, 37 °C). The tolerance limit of the cations, anions, glucose and glutathione is defined as the largest amount making the fluorescence intensity ratio (I_{528}/I_{422}) alter less than 10% (Fig. 2). Moreover, the effect of ionic strength was also investigated, and the results demonstrated that the fluorescence intensity ratio remained almost unchanged in the range of 10–200 mM PBS (RSD=1.6%, n=5) (Fig. S5). These results suggested the high selectivity of SiNDs-Apt-FAM toward pH.

3.3. Cytotoxicity assay of SiNDs-Apt-FAM

Prior to cellular imaging, the cytotoxicity of SiNDs-Apt-FAM was evaluated by the standard MTT assay (Mosmann, 1983). Briefly, MCF-7 cells were seeded in 96-well plates at a density of 1×10^4 cells/well, and incubated with SiNDs-Apt-FAM at a SiNDs concentration of 0.3–2.0 mg mL^{-1} in DMEM with 10% (v/v) fetal bovine serum and penicillin (100 units/mL)-streptomycin (100 μg mL^{-1}) liquid at 37 °C for 24 h in a 5% CO_2 incubator. The cells incubated without SiNDs-Apt-FAM were treated the same way as the control. The culture media were then abandoned, and 10 μL of the MTT solution (5 mg mL^{-1} in DMEM) was added to each well, followed by incubation for 4 h. The supernatant was discarded, and 150 μL of DMSO was then added to each well for dissolving the formed formazan. After shaking for 10 min, the absorbance was measured on a microplate reader (MK3, Thermo, USA) at 492 nm. Each concentration was tested five times. The percent of cell viability was calculated according to the following equation:

$$\text{Cell viability} = (A_{sample}-A_{blank})/(A_{control}-A_{blank}) \times 100\% \quad (2)$$

Where A_{sample} was the absorbance of the solution containing cells incubated with SiNDs-Apt-FAM, $A_{control}$ was the absorbance of the cells only, and A_{blank} was the absorbance of the PBS buffer. As indicated in

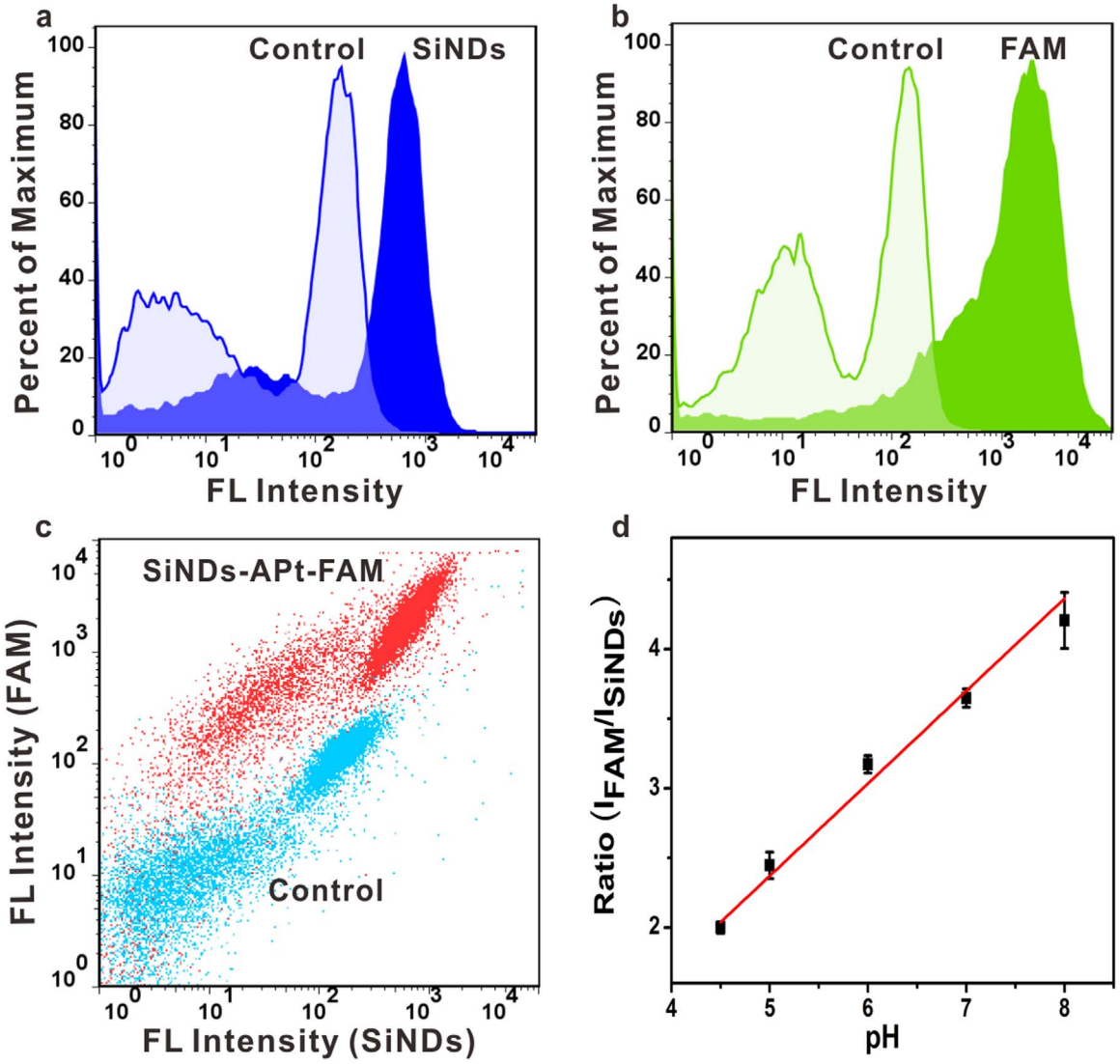

Fig. 5. Flow cytometry of MCF-7 cells incubated with SiNDs-Apt-FAM and intracellular pH calibration. Histograms are of MCF-7 cells at (a) DAPI channel for SiNDs and (b) FITC channel for FAM and are overlaid control cells incubated without SiNDs-Apt-FAM. Representative dot plot (c) for MCF-7 cells incubated with SiNDs-Apt-FAM and incubated without SiNDs-Apt-FAM (control). (d) Intracellular pH calibration curve of SiNDs-Apt-FAM.

Fig. 3, the cell viability of MCF-7 cells keeps unchanged with a high SiNDs-Apt-FAM concentration (up to 2.0 mg mL^{-1}). The corresponding concentration of the aptamer was 1.2 μM, which could not inhibit the growth of cancer cells (Liu et al., 2016). The cytotoxicity of the SiNDs-Apt-FAM was further investigated using HeLa cells with the same procedure. And the cell viability remained above 90% (Fig. S7). These results show that the aptasensor has very low toxicity for living cells detection.

3.4. Fluorescence imaging with SiNDs-Apt-FAM in living cells

For fluorescence imaging, MCF-7 cells incubated with the nanosensor exhibited obvious fluorescence signal compared to that without SiNDs-Apt-FAM (Fig. S6), indicating SiNDs-Apt-FAM entered the cells. To study the cell specificity of the multicolor imaging nanosensor, MCF-7 cells and MCF-10A normal cells were incubated with 400 μg mL^{-1} SiNDs-Apt-FAM, respectively (For more details, see Section 2). No obvious emission was observed in MCF-10A cells (Fig. 4a) and strong fluorescence could be seen in MCF-7 cells (Fig. 4b). The mean fluorescence intensity of MCF-7 cells was about 10 times higher than that of MCF-10A cells, indicating good recognition ability of the aptasensor for MCF-7 cells. To determine the subcellular localization of SiNDs-Apt-FAM in MCF-7 cells, the lysosome specific staining probe LysoTracker Red DND-99 was adopted to stain the cells with the nanosensor. MCF-7 cells were first incubated with 400 μg mL^{-1} nanosensor at 37 °C for 4 h. Cells were washed three times and then incubated with 75 nM LysoTracker Red DND-99 at 37 °C for 45 min. The application of SiNDs-Apt-FAM for fluorescence imaging was also performed using HeLa cells. In the case of MCF-7 cells, the fluorescence images of LysoTracker Red DND-99 and SiNDs-Apt-FAM could be merged well (Pearson's correlation coefficient, ρ=0.714 (red and blue images), 0.885 (red and green images)) (Fig. 4c, S9a,b), confirming that SiNDs-Apt-FAM were mainly accumulated in lysosomes and demonstrating that the aptasensor possessed good cell-membrane permeability. The degree of colocalization was comparable to that reported work relative to lysosomal imaging (Pan et al., 2016). For HeLa cells, SiNDs-Apt-FAM were distributed in lysosome and cytoplasm (Fig. S8), and the colocalization coefficients of LysoTracker Red DND-99 to the aptasensor were 0.415 (red and blue images) and 0.487 (red and green images), respectively (Fig. S9c,d). The colocalization level of the red and blue images was slightly lower than that of the red and green images for both MCF-7 cells and HeLa cells, which was probably due to the relatively high autofluorescence of cells in blue channel (Montalti et al., 2015). It is still desirable to

synthesize near-infrared-emitting silicon nanodots, which could be more favorable for cell imaging. To quantify the lysosomal hydrogen ions, MCF-7 cells were selected for the further experiment.

3.5. Fluorescence ratiometric detection of lysosomal pH with SiNDs-Apt-FAM

The tracking of pH over large cell populations is vital for understanding the general behavior of lysosome, and the successful lysosomal imaging with SiNDs-Apt-FAM inspires us to investigate the possibility of pH measurement with this ratiometric aptsensor via flow cytometry. Fig. 5a,b,c show the flow cytometry of MCF-7 cells incubated with SiNDs-Apt-FAM. The fluorescence intensity of the experimental group (i.e., cells treated by SiNDS-Apt-FAM) was much higher than the control group (i.e., cells untreated by SiNDs-Apt-FAM) (For more details, see Section 2). As the intracellular environment was different from the PBS solution in vitro, a calibration curve of pH in MCF-7 cells was obtained with H^+/K^+ ionophore nigericin, which was a standard method for equilibration of the intracellular and external pH. All data were analyzed with the mean fluorescence intensity of 1×10^4 MCF-7 cells with a excitation/emission mode. Therefore, the cells stained with SiNDS-Apt-FAM were detected by recording the blue channel emission (I_{SiNDs}) and the green channel emission (I_{FAM}) simultaneously. The intensity ratio (I_{FAM}/I_{SiNDs}) was linear against pH values from 4.5 to 8.0 in living cells [$y=0.617x - 0.984$, $R^2=0.984$] (Fig. 5d), which covered the physiological pH level (4.7–8.0) inside biological cells (Casey et al., 2010). The pH of MCF-7 cells was measured to be 5.1 ± 0.3, in accordance with the lysosomal pH value. The SiNDs-Apt-FAM aptasensor can be utilized as an effective ratiometric sensing platform for intracellular pH in living cancer cells.

4. Conclusions

A metal-free, ultrasmall, ratiometric pH aptasensor has been developed using the label-free silicon nanodots as the carrier and fluorescence reference. The new technique offers several major advantages over previously reported. First, the aptasensor can be applied to recognize cancer cells in comparison with normal cells. Second, the system is truly nontoxic, which can be used to detect analyte in cellular organelle while maintaining the cell viability. Third, intracellular chemical information can be obtained from thousands of cells simultaneously. This platform is simple, accurate for quantitative determination of pH in living cells, which may pave the way for future developments of silicon-based sensors for analysis of other biological analytes. Moreover, as the biocompatible and stable aptamer AS1411 has notably been applied in intracellular drug delivery systems associated with pH measurement, this multifunctional aptasensor based on silicon nanodots appears reliable to open broad applications in the biomedical analysis.

Acknowledgements

This work was supported by the National Natural Science Foundation of China (21475101, 21675119).

Appendix A. Supporting information

Supplementary data associated with this article can be found in the online version at doi:10.1016/j.bios.2017.03.041.

References

Albertazzi, L., Storti, B., Marchetti, L., Beltram, F., 2010. J. Am. Chem. Soc. 132, 18158–18167.
Bao, Y.Y., De Keersmaecker, H., Corneillie, S., Yu, F., Mizuno, H., Zhang, G.F., Hofkens, J., Mendrek, B., Kowalczuk, A., Smet, M., 2015. Chem. Mater. 27, 3450–3455.
Cao, C., Zhang, J., Wen, X., Dodson, S.L., Dao, N.T., Wong, L.M., Wang, S., Li, S., Phan, A.T., Xiong, Q., 2013. ACS Nano 7, 7583–7591.
Casey, J.R., Grinstein, S., Orlowski, J., 2010. Nat. Rev. Mol. Cell Biol. 11, 50–61.
Chan, Y.H., Wu, C., Ye, F., Jin, Y., Smith, P.B., Chiu, D.T., 2011. Anal. Chem. 83, 1448–1455.
Chen, C.H., Xiang, X., Liu, Y.F., Zhou, G.H., Ji, X.H., He, Z.K., 2014. Biosens. Bioelectron. 58, 205–208.
Chen, Y.C., Zhu, C.C., Cen, J.J., Bai, Y., He, W.J., Guo, Z.J., 2015. Chem. Sci. 6, 3187–3194.
Dasog, M., Kehrle, J., Rieger, B., Veinot, J.G.C., 2016. Angew. Chem. Int. Ed. 55, 2322–2339.
Dennis, A.M., Rhee, W.J., Sotto, D., Dublin, S.N., Bao, G., 2012. ACS Nano 6, 2917–2924.
Feng, Y.L., Liu, Y.F., Su, C., Ji, X.H., He, Z.K., 2014. Sens. Actuators B 203, 795–801.
Gong, P., Yang, Y.T., Yi, H.Q., Fang, S.T., Zhang, P.F., Sheng, Z.H., Gao, G.H., Gao, D.Y., Cai, L.T., 2014. Nanoscale 6, 5416–5424.
Gu, L., Hall, D.J., Qin, Z.T., Anglin, E., Joo, J., Mooney, D.J., Howell, S.B., Sailor, M.J., 2013. Nat. Commun. 4.
Han, J.Y., Burgess, K., 2010. Chem. Rev. 110, 2709–2728.
He, C., Lu, K., Lin, W., 2014. J. Am. Chem. Soc. 136, 12253–12256.
Ji, X.Y., Peng, F., Zhong, Y.L., Su, Y.Y., Jiang, X.X., Song, C.X., Yang, L., Chu, B.B., Lee, S.T., He, Y., 2015. Adv. Mater. 27, 1029–1034.
Kosegarten, H., Englisch, G., 1994. J. Plant Nutr. Soil Sc. 157, 401–405.
Li, J., Zhong, X., Cheng, F., Zhang, J.R., Jiang, L.P., Zhu, J.J., 2012. Anal. Chem. 84, 4140–4146.
Li, J., Hong, C.Y., Wu, S.X., Liang, H., Wang, L.P., Huang, G., Chen, X., Yang, H.H., Shangguan, D., Tan, W., 2015. J. Am. Chem. Soc. 137, 11210–11213.
Liu, J., Wei, T., Zhao, J., Huang, Y.Y., Deng, H., Kumar, A., Wang, C.X., Liang, Z.C., Ma, X.W., Liang, X.J., 2016. Biomaterials 91, 44–56.
Marin, M.J., Galindo, F., Thomas, P., Russell, D.A., 2012. Angew. Chem. Int. Ed. 51, 9657–9661.
Montalti, M., Cantelli, A., Battistelli, G., 2015. Chem. Soc. Rev. 44, 4853–4921.
Mosmann, T., 1983. J. Immunol. Methods 65, 55–63.
Nie, H., Li, M.J., Li, Q.S., Liang, S.J., Tan, Y.Y., Sheng, L., Shi, W., Zhang, S.X.A., 2014. Chem. Mater. 26, 3104–3112.
Pan, W., Wang, H.H., Yang, L.M., Yu, Z.Z., Li, N., Tang, B., 2016. Anal. Chem. 88, 6743–6748.
Patrick, M.J., Janjic, J.M., Teng, H., O'Hear, M.R., Brown, C.W., Stokum, J.A., Schmidt, B.F., Ahrens, E.T., Waggoner, A.S., 2013. J. Am. Chem. Soc. 135, 18445–18457.
Qiu, L.P., Wu, C.C., You, M.X., Han, D., Chen, T., Zhu, G.Z., Jiang, J.H., Yu, R.Q., Tan, W.H., 2013. J. Am. Chem. Soc. 135, 12952–12955.
Shangguan, J., He, D., He, X., Wang, K., Xu, F., Liu, J., Tang, J., Yang, X., Huang, J., 2016. Anal. Chem. 88, 7837–7843.
Shi, W., Li, X.H., Ma, H.M., 2012. Angew. Chem. Int. Ed. 51, 6432–6435.
Shieh, Y.A., Yang, S.J., Wei, M.F., Shieh, M.J., 2010. ACS Nano 4, 1433–1442.
Turk, B., Turk, V., 2009. J. Biol. Chem. 284, 21783–21787.
Vidal-Donet, J.M., Carcel-Trullols, J., Casanova, B., Aguado, C., Knecht, E., 2013. PLoS One 8.
Wan, Q., Chen, S., Shi, W., Li, L., Ma, H., 2014. Angew. Chem. Int. Ed. 53, 10916–10920.
Wang, J., Ye, D.X., Liang, G.H., Chang, J., Kong, J.L., Chen, J.Y., 2014. J. Mater. Chem. B 2, 4338–4345.
Wang, X., Song, P., Peng, L., Tong, A., Xiang, Y., 2016. ACS Appl. Mater. Inter. 8, 609–616.
Wencel, D., Abel, T., McDonagh, C., 2014. Anal. Chem. 86, 15–29.
Wu, L., Li, X., Huang, C., Jia, N., 2016. Anal. Chem. 88, 8332–8338.
Wu, M.Y., Li, K., Liu, Y.H., Yu, K.K., Xie, Y.M., Zhou, X.D., Yu, X.Q., 2015. Biomaterials 53, 669–678.
Xu, J.Q., Sun, L., Li, J., Liang, J.L., Zhang, H.M., Yang, W.S., 2011. Nanoscale Res. Lett. 6, 1–7.
Zhang, P.H., Cheng, F.F., Zhou, R., Cao, J.T., Li, J.J., Burda, C., Min, Q.H., Zhu, J.J., 2014. Angew. Chem. Int. Ed. 53, 2371–2375.
Zhao, D., Chan, W.H., He, Z.K., Qiu, T., 2009. Anal. Chem. 81, 3537–3543.
Zhong, Y., Sun, X., Wang, S., Peng, F., Bao, F., Su, Y., Li, Y., Lee, S.T., He, Y., 2015. ACS Nano 9, 5958–5967.
Zhou, J., Yang, Y., Zhang, C.Y., 2015. Chem. Rev. 115, 11669–11717.